



Polymer Degradation and Stability

Polymer Degradation and Stability 90 (2005) 123-131

www.elsevier.com/locate/polydegstab

# Biopolymer chitosan/montmorillonite nanocomposites: Preparation and characterization

S.F. Wang a,\*, L. Shen a, Y.J. Tong b, L. Chen a, I.Y. Phang a, P.Q. Lim a, T.X. Liu a

Institute of Materials Research and Engineering, A\*STAR, 3 Research Link, Singapore 117602, Singapore
 Fujian Normal University, Department of Chemistry, Fuzhou 350007, People's Republic of China

Received 13 January 2005; received in revised form 1 March 2005; accepted 6 March 2005 Available online 25 April 2005

#### Abstract

Biopolymer chitosan/montmorillonite nanocomposites have been prepared in which montmorillonite (MMT) is used as nanofiller and diluted acetic acid is used as solvent for dissolving and dispersing chitosan and montmorillonite. Morphology and properties of chitosan nanocomposites with and without acetic acid residue have been studied compared with those of pure chitosan. The effect of acetic acid residue and MMT loading in nanocomposites has been investigated. The XRD and TEM results indicate the formation of an intercalated-and-exfoliated nanostructure at low MMT content and an intercalated-and-flocculated nanostructure at high MMT content. The thermal stability and the mechanical properties of the nanocomposites are characterized by TGA and nanoindentation. The nano-dispersed clay improves the thermal stability and enhances the hardness and elastic modulus of the matrix systematically with the increase of clay loading. The existence of acetic acid residue in chitosan matrix will affect its crystallinity, thermal stability and mechanical properties.

© 2005 Elsevier Ltd. All rights reserved.

Keywords: Chitosan; Montmorillonite; Nanocomposites; Structure; Thermal properties; Nanoindentation

#### 1. Introduction

The traditional non-biodegradable polymers, which are produced from fossil fuels, have considerably disturbed and damaged the ecosystem of nature. For this reason there is an urgent need to develop renewable source-based biopolymer materials that would not involve the use of toxic or noxious components in their manufacture and could allow degradation via a natural composting process. Polylactide and polysaccharides are most promising candidates because they are made or come from naturally abundant products and are readily biodegradable. However, in order to render biopolymers able to compete with stronger and more ductile

commodity polymers such as polyethylene or polypropylene, there is still a need to improve their properties including thermal stability, mechanical properties and barrier properties. At this point it is noteworthy to point out that polymer-layer silicate nanocomposite (PLSNs) technology has already proven to be a good way to improve these properties significantly [1–8]. Although much attention has been paid to polymer/clay nanocomposites, relatively little attention has been paid to biopolymer/clay nanocomposites. These are the cases of polylactide/clay nanocomposites [8,9], cotton/clay nanocomposites [10], poly(butylenes succinate)/clay nanocomposites [11] and plant oils/clay nanocomposites [12].

Chitosan, a polysaccharide composed mainly of  $\beta$ -(1,4)-linked 2-deoxy-2-amino-D-glucopyranose units, is the deacetylated product of chitin, poly(N-acetyl-D-glucopyranose. Chitosan and chitin, next to cellulose, are the second most plentiful natural biopolymers.

<sup>\*</sup> Corresponding author. Tel.: +65 68748196; fax: +65 67741042.

E-mail address: sf-wang@imre.a-star.edu.sg (S.F. Wang).

Chitosan has been extensively investigated for several decades for molecular separation, food packaging film, artificial skin, bone substitutes, water engineering and so on, owing to its good mechanical properties, biocompatibility, biodegradability, multiple functional groups as well as solubility in aqueous medium [15]. However, its properties, such as thermal stability, hardness and gas barrier properties are frequently not good enough to meet those wide ranges of applications. Up to now, there is only a limited number of reports about the enhancement of properties of chitosan using PLSNs technology [13,14]. Asira had a preliminary study about chitosan clay nanocomposites and reported a markedly improved tensile property but inferior thermal property of composites to that of pure chitosan [13]. Ruiz-Hitzky and his coworkers synthesized functional chitosan/ montmorillonite nanocomposites, which can effectively act as active phase for an electrochemical sensor in the detection of different anions [14]. All of them prepared nanocomposites by exfoliation—adsorption method, which used diluted acetic acid solvent for dispersing and dissolving clay and chitosan. However, there are few reports about the effect of acetic acid residue on the effect of chitosan nanocomposites, and the effect of hydrogen bond between chitosan and MMT, which may be the key driving force to make the MMT layers assemble to form flocculated structure in chitosan matrix.

Taking these antecedents into account, the aim of the present study is to prepare high-performance chitosan by incorporating montmorillonite at the nanometre scale. The effects of acetic acid residue, the hydrogen bonding force between chitosan and MMT and clay loading on the morphology, thermal stability and mechanical properties of the nanocomposites have been investigated.

## 2. Experimental

#### 2.1. Materials

Chitosan (CS) of medium molecular weight (average molecular weight  $M_{\rm v} = 92,700~{\rm g~mol}^{-1}$ ), used in this work was bought from Aldrich Chemicals. This chitosan was obtained by deacetylation of chitin from crab shells and it had a degree of deacetylation of 82.5%. Glacial acetic acid (HAc) obtained from Aldrich Chemicals was used as the solvent for chitosan. The unmodified pristine montmorillonite (MMT), with a cationic exchange capacity (CEC) of 92.7 mequiv/100 g, was supplied by Nanocor Inc.

## 2.2. Preparation of the nanocomposites

HAc-CS/MMT nanocomposites: chitosan solution was prepared by dissolving chitosan (CS) in a 2% (v/v) aqueous acetic acid solution at a concentration of

2 wt% followed by centrifuging to remove the insoluble material. MMT was first swelled by 50 ml distilled water and then added to 50 ml chitosan solution with MMT contents of 2.5 wt%, 5 wt%, 10 wt%, followed by stirring at 60 °C for 6 h. After that, MMT/CS solutions were cast on a plastic dish at 60 °C for 48 h. The dry films still contained a small quantity of the solvent (HAc), which formed chitosonium acetate, and they were termed HAc-CS-x (x is concentration of MMT).

CS/MMT nanocomposites: CS/MMT nanocomposites were prepared by the same procedure as HAc-CS/MMT nanocomposites. After drying, the films were soaked in 1 M aqueous NaOH for 5 h to neutralize the acid followed by rinsing in distilled water to neutral and then dried at 60 °C for 24 h. They were termed CS-x (x is the content of MMT).

All the nanocomposite films were dried at 80 °C for overnight before testing and the neat HAc-CS and CS films were made in the same conditions as their nanocomposites. The thermal stability and mechanical properties of chitosan and the nanocomposites with and without the residue of HAc were compared.

#### 2.3. XRD and TEM

Wide-angle X-ray diffraction (XRD) patterns of the sheet samples were recorded using a Bruker GADDS diffractometer with area detector operating at a voltage of 40 kV and a current of 40 mA using Cu K $\alpha$  radiation ( $\lambda = 0.15418$  nm). Ultrathin films (with thickness of about 80 nm) for transmission electron microscopy (TEM) observation were prepared by cutting from the epoxy block with the embedded nanocomposite sheet at room temperature using a Leica ultramicrotome with a diamond knife. The TEM micrographs were taken using a Philips CM300-FEG transmission electron microscope under an accelerating voltage of 150 kV. Sections were observed with 200-mesh carbon coated copper grids without any further modification or coating.

#### 2.4. FTIR

Fourier transform infrared (FTIR) spectra (transmission) were measured on a Perkin-Elmer FTIR spectrophotometer 2000 in the range of 4000–400 cm<sup>-1</sup> at a resolution of 4 cm<sup>-1</sup>.

#### 2.5. Thermal analysis

The thermal properties of nanocomposites and pure chitosan were investigated by thermogravimetric analysis (TGA). TGA was performed under nitrogen and air flows from room temperature to 800 °C at a rate of 20 °C/min with a TA TGA 2050 instrument. The weights of samples varied from 5 to 8 mg.

#### 2.6. Nanoindentation experiments

The nanoindentation tests were performed with an MTS Nano Indenter® XP (MTS Cooperation, Nano Instruments Innovation Center, TN, USA) with a continuous stiffness measurement (CSM) technique [16]. The CSM technique used in the present study was accomplished by imposing an oscillated force with known frequency and amplitude on top of the nominal applied force. The material's displacement response at the excitation frequency is recorded continuously as a function of the indentation depth. The material's stiffness (S) and damping ( $\omega C$ ) along the indentation loading can be solved by using Eqs. (1) and (2), respectively. The hardness and elastic modulus are calculated from Eqs. (3) and (4), respectively. Therefore, the hardness and modulus are determined as a function of indentation depth.

$$S = \left[\frac{1}{\frac{P_{\text{max}}}{h(\omega)}\cos\Phi - (K_{\text{s}} - m\omega^2)} - K_{\text{f}}^{-1}\right]^{-1}$$
(1)

$$\omega C = \frac{P_0}{h(\omega)} \sin \Phi \tag{2}$$

$$\frac{E}{1-\nu^2} = \frac{\sqrt{\pi}}{2} \frac{1}{\sqrt{A_c}} S \tag{3}$$

$$H = \frac{P_{\text{max}}}{A_{\text{c}}} \tag{4}$$

 $P_{\rm max}$  and  $h(\omega)$  are driving force and the displacement response of the indenter, respectively;  $\Phi$  is the phase angle between  $P_{max}$  and  $h(\omega)$ ; m is mass of the indenter column;  $K_{\rm s}$  is the spring constant in the vertical direction;  $K_{\rm f}$  is frame stiffness; m,  $K_{\rm s}$  and  $K_{\rm f}$  are all constant values for specified indentation system.  $\omega$  is angular speed which equals to  $2\pi f$ ; f is the driven frequency of the AC signal.  $\nu$  is Possion's ratio and set to be 0.35 for the current analysis [17].  $A_{\rm c}$  is contact area at the moment the material is in contact with indenter with load  $P_{\rm max}$ .

A three-sided pyramidal (Berkovich) diamond indenter was employed for the indentation experiments. The area function, which is used to calculate contact area  $A_{\rm c}$  from contact depth  $h_{\rm c}$ , was carefully calibrated using standard sample, fused silica, before the experiments. Chitosan and its clay nanocomposite films with thickness of approximately 60  $\mu$ m were mounted on flat aluminium stubs by super glue. In the indentation test, the indenter was pressed into the materials with a constant strain rate, i.e.  $0.05 \, 1/s$ , from sample surface to 3000 nm deep into the surface. The maximum load was then held constant for 60 s in order to monitor the

creep behaviour of the material. Finally, the indenter was withdrawn from the surface with same rate as loading until 10% of the maximum load. Here, constant strain rate was chosen to load on the samples in order to avoid strain-hardening effect on the measurements [18]. At least 20 indents were performed on each sample and the interval of each two indents was 50  $\mu$ m to avoid interaction.

#### 3. Results and discussion

#### 3.1. Nanostructure and morphology

The clay dispersion within chitosan has been characterized by both XRD and TEM, which are the most frequently used methods to study the structure of nanocomposites. Depending on the relative distribution/dispersion of the stacks of clay platelets, three types of PLSN can be described [2,3]: intercalated PLSNs, where polymer chains are intercalated into the silicate layers resulting in a well ordered mutilayer morphology built up with alternating polymer and inorganic layers; flocculated PLSNs, where intercalated stacked silicate layers are sometime flocculated due to the hydroxylated edge—edge interactions, and exfoliated/delaminated PLSNs, where the silicate layers are completely homogenously dispersed in the polymer matrix.

Because of the hydrophilic and polycationic nature of chitosan in acidic media, this biopolymer has good miscibility with MMT and can easily intercalate into the interlayers by means of cationic exchange [14]. The clay dispersion within chitosan has been characterized by both XRD and TEM. Fig. 1a illustrates the XRD patterns of MMT, neat CS and its CS/MMT nanocomposites with different MMT concentrations. The XRD pattern of the MMT shows a reflection peak at about  $2\theta = 7.1^{\circ}$ , corresponding to a basal spacing of 1.25 nm. The XRD pattern of CS shows the characteristic crystalline peaks at around  $2\theta = 10^{\circ}$ ,  $20^{\circ}$  and  $25^{\circ}$ . According to the reports [19,20], the peaks around 10° and 20° are related to crystal (1) and crystal (2) in chitosan, respectively. The unit cell of crystal (1) is characterized by a = 7.76, b = 10.91, c = 10.30 Å, and  $\beta = 90^{\circ}$ , and it is larger than that of crystal (2), whose unit cell is characterized by a = 4.4, b = 10.0, c = 10.30 Å, and  $\beta = 90^{\circ}$ . After incorporating MMT within CS, the basal plane of MMT at  $2\theta = 7.1^{\circ}$ disappears, substituted by a new weakened broad peak at around  $2\theta = 3-5^{\circ}$ . The movement of the basal reflection of MMT to lower angle indicates the formation of an intercalated nanostructure, while the peak broadening and intensity decreases most likely indicate the disordered intercalated or exfoliated structure. However, it is difficult for XRD to give definitive conclusions about the defined structure. Thus, TEM

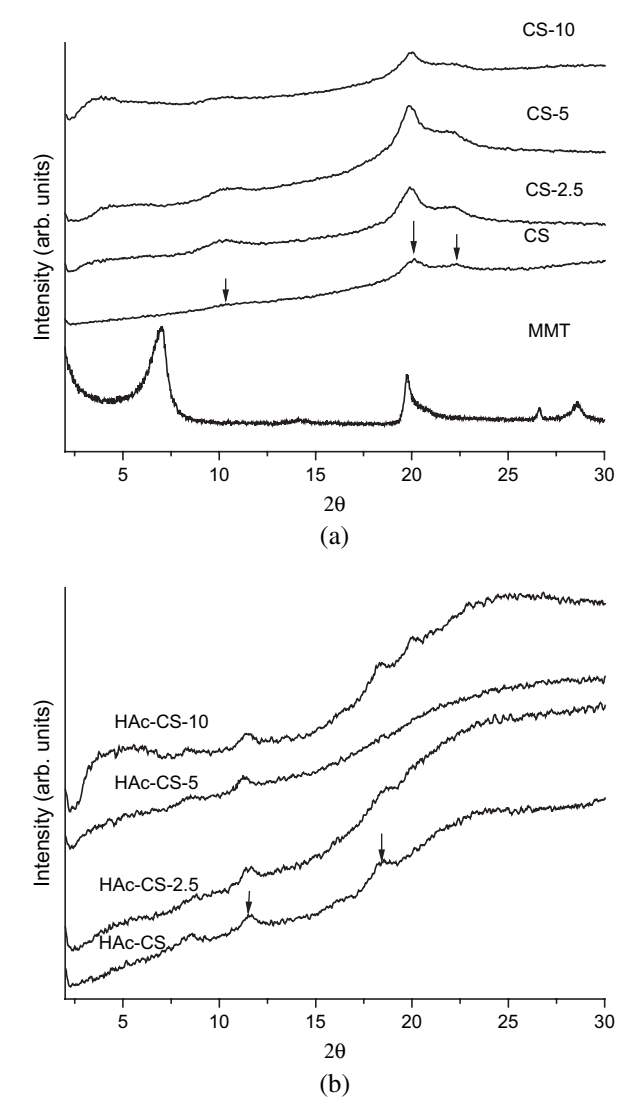


Fig. 1. XRD patterns of: (a) the montmorillonite (MMT), pure chitosan (CS), and its nanocomposites with MMT/CS ratios of 2.5% (CS-2.5), 5% (CS-5) and 10% (CS-10); (b) HAc-CS and its nanocomposites with MMT/HAc-CS ratios of 2.5% (HAc-CS-2.5), 5% (HAc-CS-5) and 10% (HAc-CS-10); the arrow marks the peak position.

techniques are necessary to characterize the morphology of the nanocomposites. All the TEM images show the good dispersion of MMT in the CS matrix. At lower MMT content (2.5 wt%, Fig. 2a), the MMT shows the coexistence of both intercalated (stacks of multilayers of MMT) and exfoliated structures. This result is consistent with the result of XRD. With increasing the content of the MMT (5 wt%, Fig. 2b, c, and 10 wt% Fig. 2d), the MMT clearly shows intercalated morphology with occasional floculation. The size of some stacks of MMT layers appears to reach about 400–600 nm. The stacks of MMT layers connect with each other edge by edge and form floculated structure. The appearance of the d<sub>001</sub> peak at 3–5° indicates the formation of partly order-intercalated structure. Thus, on the base of XRD

patterns and TEM images, it is clearly illustrated that the MMT keeps intercalated and exfoliated structures at lower MMT content, while with the increasing of MMT content, the MMT layers assemble to form intercalated and flocculated structures. It is believed that the formation of flocculated structure in CS/MMT nanocomposites is due to the hydroxylated edge—edge interaction of the silicate layers [11]. Since one chitosan unit possesses one amino and two hydroxyl functional groups, these functional groups can form hydrogen bonds (see Scheme 1) with the silicate hydroxylated edge groups, which lead to the strong interaction between matrix and silicate layers. This strong interaction is believed to be the main driving force for the assembly of MMT in the CS matrix to form flocculated structure.

For those chitosans containing HAc residue, Fig. 1b illustrates the XRD patterns of HAC-CS and its HAc-CS/MMT nanocomposites with different MMT concentrations. The HAc-CS exhibits two weak crystalline peaks at  $2\theta = 11.5^{\circ}$  and  $2\theta = 18.5^{\circ}$  with a strong broad slope around  $2\theta = 25^{\circ}$ , indicating the formation of an amorphous structure. Comparing Fig. 1a with Fig. 1b, clearly shows that CS without HAc residue shows higher crystallinity than that of chitosan film containing HAc residue (HAc-CS). The lower crystallinity of HAc-CS is ascribed to the presence of HAc solvent residue, which may hinder the formation of inter- and intramolecular hydrogen bonds in CS and result in less packing. In contrast to chitosan, the addition of MMT has little change in the crystallinity of chitosan, as supported by the XRD patterns where CS/MMT nanocomposites still keep the characteristic peaks of chitosan. The presence of chitosonium acetate in HAc-CS samples was also proved from FTIR spectra. Fig. 3 shows the FTIR spectra for CS, CS-5 and HAc-CS, HAc-CS-5. HAc-CS and HAc-CS-5 clearly show the peak at 1558 cm<sup>-1</sup>, which corresponds to the deformation vibration of the protonated amine group (-NH<sub>3</sub><sup>+</sup>Ac<sup>-</sup>) in chitosan, while CS and CS-5 show the peak at 1587 cm<sup>-1</sup>, which corresponds to the  $-NH_2$  band.

This complexity of clay morphologies among matrices and the different crystallinities of CS and HAc-CS will definitely affect the thermal and mechanical properties of the final products.

# 3.2. Thermal stability

The thermal stability of the chitosan (CS and HAc-CS) and its nanocomposites has been investigated by TGA under both nitrogen and air flows (Fig. 4). On the TGA curves, one can see that the degradation of chitosan and its nanocomposite in the nitrogen and air flows is different. Under nitrogen flow, a non-oxidative degradation occurs, while the use of air allows oxidative degradation of the samples. Under nitrogen flow, there are two steps of degradation. The first range

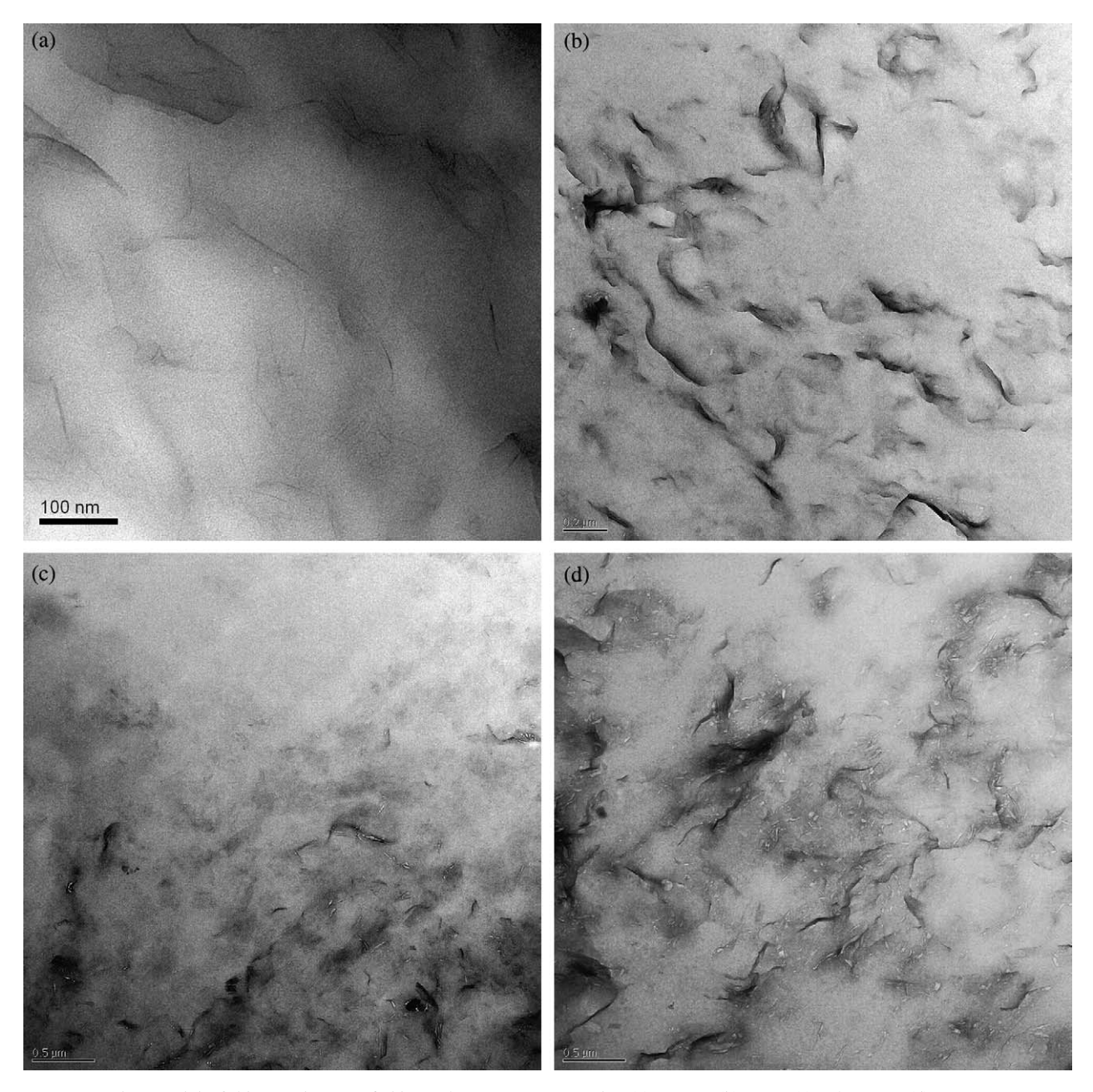


Fig. 2. Bright field TEM images of chitosan/MMT nanocomposite: (a) CS-2.5; (b) CS-5; (c) HAc-CS-5; (d) CS-10.

(50–200 °C) is associated with the loss of water about 5–8 wt%, whereas the second range (200–450 °C) corresponds to the degradation and deacetylation of chitosan and left about 50 wt% solid residue. This is similar to the results reported by other researchers [21,22]. In air flow, there is another degradation step (450–700 °C), which may be assigned to the oxidative degradation of the carbonaceous residue formed during the second step. From Fig. 4a–d and Table 1 it is clearly observed that the degradation mechanism of CS and its nanocomposites is somehow different from the HAc-CS and its nanocomposites decompose faster and thoroughly and thus are less stable

than those of CS and its nanocomposites. The residue of HAc in chitosan strongly induces the thermal degradation of the matrix. A similar phenomenon was also observed by Glasser and his coworkers [23]. They recorded a progressive loss of mass below 250 °C, the temperature at which chitin and chitosan began to thermally degrade, when powdered chitosonium acetate was exposed to heating by TGA.

The nano-dispersed clay in the chitosan matrix exhibits a significant delay in weight loss, especially at high temperature (>400 °C). After pyrolysis, the nanocomposite forms char with a multilayered carbonaceous-silicate structure, which may keep its multilayered

Scheme 1. Formation of hydrogen bonds between chitosan and MMT.

structure in the polymer matrix even at 600 °C [24]. This high-performance carbonaceous-silicate char builds up on the surface during burning, thus insulating the underlying material and slowing the escape of the volatile products generated during decomposition. As the decomposition temperature at 50% weight loss is concerned, both CS/MMT and HAc-CS/MMT nanocomposites show higher thermal stability compared to those of the pure CS and HAc-CS. When 50% weight

loss was selected as a measuring point, CS/MMT nanocomposites with 2.5 wt% to 10 wt% MMT can be 25 °C to 100 °C higher than that of pure CS; while HAc-CS/MMT nanocomposites with 2.5 wt% to 10 wt% MMT only exhibit 10 °C to 30 °C higher than that of pure HAc-CS. Nanocomposites have 2–8 wt% higher char residue at 750 °C in accordance to the addition of MMT, which is extremely thermally stable and shows more than 90% solid residue at 750 °C. The clay acts as

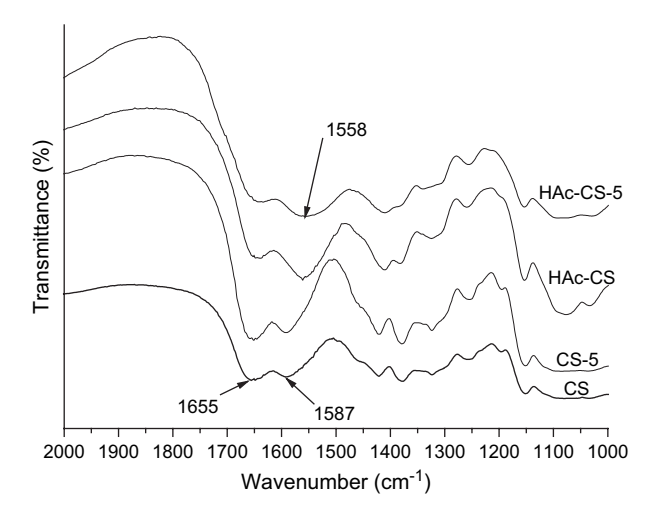


Fig. 3. FTIR spectrum of: (A) CS, (B) CS-5, (C) HAc-CS and (D) HAc-CS-5.

a heat barrier as well as assists in the formation of char after thermal decomposition. The nano-dispersed lamellae of clay in polymer matrix will result qualitatively in a spatially more uniform and thicker char during decomposition. The nano-dispersed clay enhances the formation of char on the surface of polymer matrix and as a consequence, reduces the rate of decomposition [25,26]. The thermal stability of the nanocomposites increases systematically with increasing clay, up to loading of 10 wt%. Our results are contrary to the report of Fuongfuchat [13], who observed inferior thermal properties of composites to that of pure chitosan. The difference may be due to the fact that we choose different chitosans with different degree of acetylation.

#### 3.3. Nanoindentation experiments

The modulus and hardness profiles along the indentation direction of the CS, HAc-CS and their nanocomposites are shown in Fig. 5(A), (B) and Fig. 6(A), (B), respectively. In general, the moduli of the nanocomposites are higher than the pure system as shown in Fig. 5(A) and Fig. 6(A). Increasing the clay concentration in the nanocomposite has improved the stiffness of the material significantly at a similar indentation depth. It is interesting to notice that, for the nanocomposites with higher clay concentration, i.e., 5 wt% and 10 wt%, the modulus profile is shifting

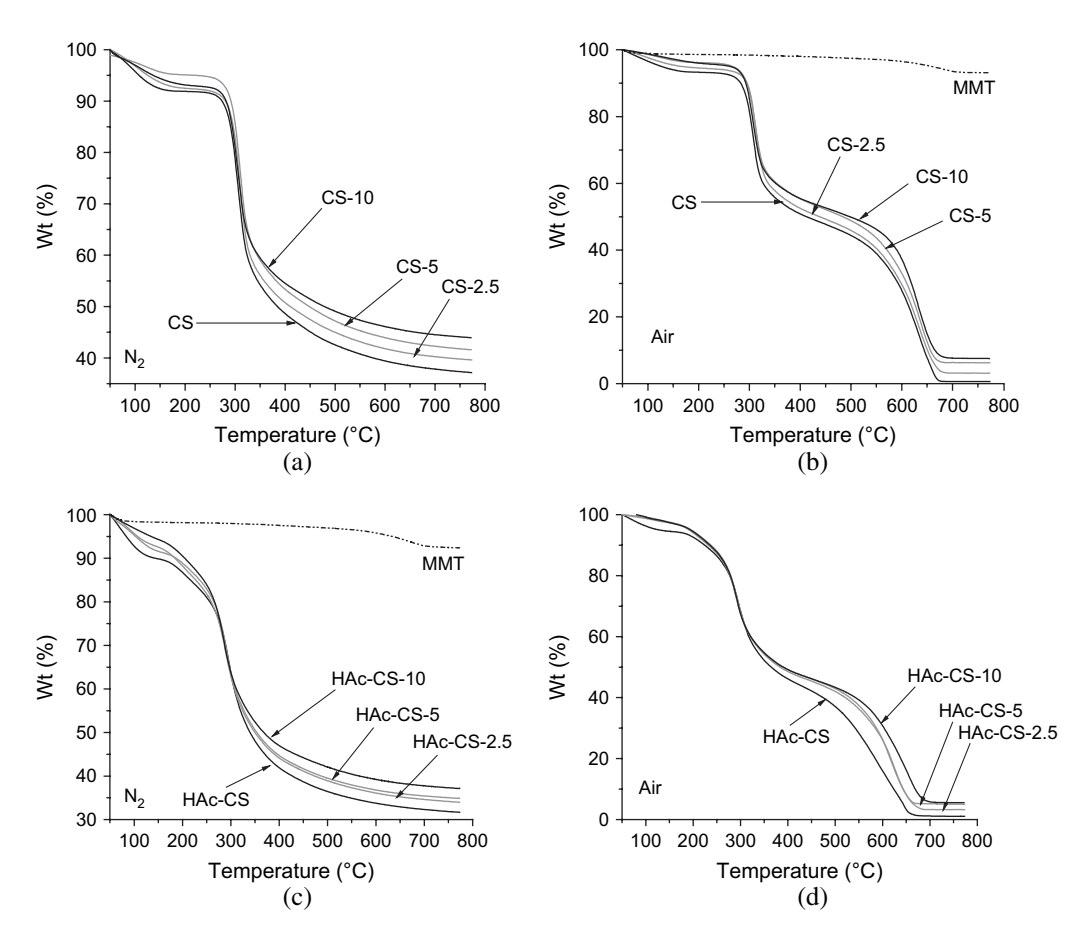


Fig. 4. Thermogravimetric curves of montmorillonite, chitosan and its nanocomposites: (a) CS, CS-2.5, CS-5 and CS-10 in nitrogen flow; (b) MMT, CS, CS-2.5, CS-5 and CS-10 in air flow; (c) MMT, HAc-CS, HAc-CS-2.5, HAc-CS-5 and HAc-CS-10 in nitrogen flow; (d) HAc-CS, HAc-CS-2.5, HAc-CS-5 and HAc-CS-10 in air flow.

Table 1 Peak temperature and weight loss in TG during the thermal degradation of chitosan and its nanocomposites in both nitrogen and air flows

Samples	Temperature at 20 wt% loss (°C)		Temperature at 50 wt% loss (°C)		Char at 750 °C (wt%)	
	$\overline{N_2}$	Air	$N_2$	Air	$N_2$	Air
CS	298	301	385	412	37.3	0.6
CS-2.5	303	309	410	438	39.8	3.2
CS-5	306	309	448	484	41.8	6.7
CS-10	301	305	479	497	44.1	7.6
HAc-CS	256	277	339	365	31.9	1.1
HAc-CS-2.5	259	279	349	375	34.2	3.3
HAc-CS-5	265	277	353	380	35.1	5.1
HAc-CS-10	267	278	368	390	37.3	5.6

neat chitosan and that with 2.5 wt% of clay show only slight modulus increment in the depth range up to 3000 nm, it is believed that the modulus increment for

upwards with increasing indentation depth. Since the

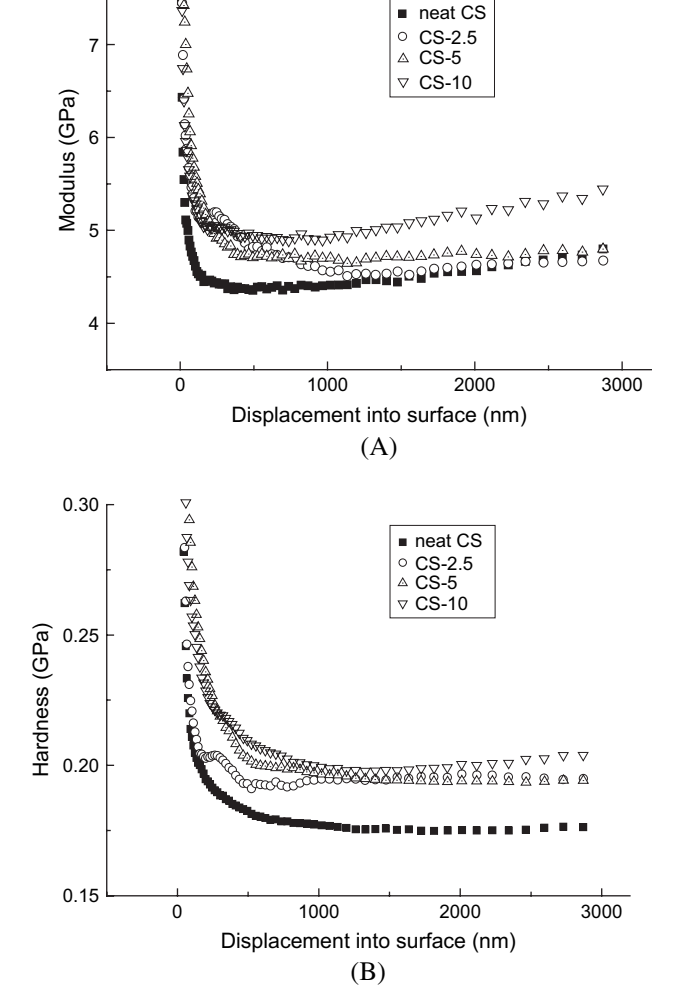


Fig. 5. Nanoindentation experiments. Hardness and modulus profiles of CS as a function of clay loading. (A) Modulus profile; and (B) hardness profile.

the nanocomposites with higher clay loading is probably due to the effect of inhomogeneous clay dispersion on the polymer properties. This phenomenon reminds us of previous reports on nylon-6/clay nanocomposites [27,28], in which a gradient distribution of nanoclay induced by injection-moulding was clearly shown by optical microscopy, XRD and thermal analysis. With higher clay loading in the matrix, the possibility of inhomogeneous distribution of clay is larger. The relative stable modulus profile of the nanocomposite with 2.5 wt% clay indicates that, among the three nanocomposites, the sample with this concentration has a more homogeneous dispersion of clay than those with higher concentrations. It is worth to note that, with increasing indentation depth, indenter may 'feel' the effect from substrate, i.e. the aluminium stub for present study, after certain indentation depth [29,30]. Therefore, to avoid the substrate effect on the modulus measurement, the minimum values in each profile, i.e., averaged values

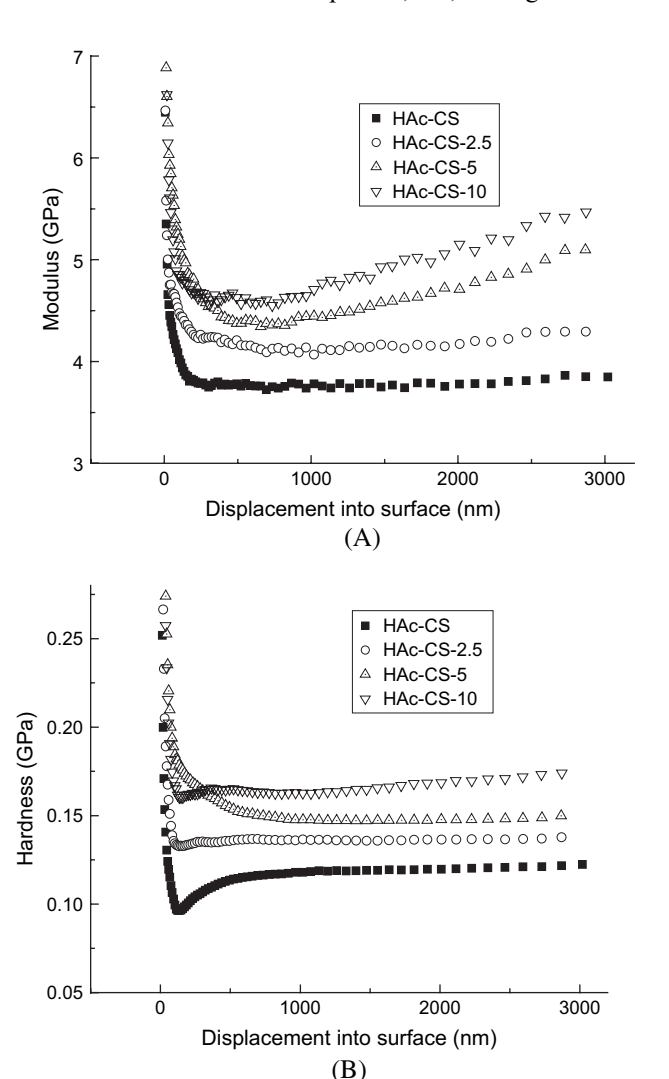


Fig. 6. Nanoindentation experiments. Hardness and modulus profiles of HAc-CS as a function of clay loading. (A) Modulus profile; and (B) hardness profile.

Table 2 Summary of the average values of elastic modulus and hardness of chitosan and its nanocomposites as a function of clay concentration

Samples	Modulus (GPa) (500–1000 nm)	Hardness (GPa) (1000–2000 nm)	
With HAc			
HAc-CS	$3.76 \pm 0.15$	$0.119 \pm 0.006$	
HAc-CS-2.5	$4.13 \pm 0.09$	$0.136 \pm 0.002$	
HAc-CS-5	$4.39 \pm 0.20$	$0.147 \pm 0.008$	
HAc-CS-10	$4.74 \pm 0.34$	$0.164 \pm 0.009$	
Without Hac			
CS	$4.39 \pm 0.06$	$0.176 \pm 0.004$	
CS-2.5	$4.69 \pm 0.15$	$0.195 \pm 0.008$	
CS-5	$4.71 \pm 0.47$	$0.195 \pm 0.022$	
CS-10	$4.92 \pm 0.41$	$0.199 \pm 0.023$	

in the depth range from 500 nm to 1000 nm are reported to represent the properties of the materials. The summarized modulus and hardness for the neat and nanocomposites samples are listed in Table 2. It is shown that, with addition of 2.5 wt% of clay, the moduli of CS-2.5 and HAc-CS-2.5 nanocomposites have increased by approximately 6.8% and 9.8%, respectively, comparing with their neat counter parts. With addition of 10 wt% of clay, the moduli of CS-10 and Hac-CS-10 dramatically increased for about 12% and 26.1%, respectively, indicating that clay addition has effectively enhanced the stiffness of the chitosan system.

The effect of clay loading on the hardness of chitosan nanocomposites is similar to that on modulus as shown in Fig. 5(B) and Fig. 6(B). In Table 2, the representative range for hardness is chosen to be from 1000 nm to 2000 nm, since the hardness shows to be more stable at this range than that shown in shallower range. The dramatic change of hardness and modulus at the very top surface, i.e., less than 500 nm, might be due to the indentation size effect (ISE), as explained elsewhere [31].

Higher modulus and hardness are found for CS and its nanocomposites, however, with increase of MMT loading, the difference between CS/MMT and HAc-CS/MMT becomes smaller. The lower mechanical properties of HAc-CS are most probably due to its lower crystallinity. The residue of HAc solvent in CS hinders the formation of hydrogen bonds in CS, which results in the higher amorphous area in CS.

#### 4. Conclusions

A mixed structure from exfoliated—intercalated to intercalated—flocculated biopolymer chitosan/clay nanocomposites has been prepared by exfoliation—adsorption method. TGA shows that the thermal stability of the CS-10 nanocomposites is improved, being 94.3 °C and 85.5 °C higher in decomposition temperature at 50% weight loss in nitrogen and air

flows, respectively. It shows that the hardness and the elastic modulus are gradually enhanced with increasing clay concentration. Furthermore, compared to the CS and its nanocomposites and HAc-CS and its nanocomposites, the former have superior thermal stability and modulus as well as hardness to the later ones. The existence of acetic acid (HAc) would induce thermal decomposition of CS matrix and decrease the crystal-linity of the CS.

#### References

- [1] Giannelis EP. Adv Mater 1996;8:29.
- [2] Alexandre M, Dubois P. Mater Sci Eng R 2000;28:1.
- [3] Ray SS, Okamoto M. Prog Polym Sci 2003;28:1539.
- [4] Ruiz-Hitzky E. Chem Rec 2003;3:88.
- [5] Kawasumi MJ. Polym Sci A Polym Chem 2004;42:819.
- [6] Kojima Y, Usuki A, Kawasumi M, Okada A, Fukushima K, Kurauchi T, et al. J Mater Res 1993;8:1185.
- [7] Wang SF, Hu Y, Zong RW, Tang Y, Cheng ZY, Fan WC. Appl Clay Sci 2004;25:49.
- [8] Maiti P, Yamada K, Okamoto M, Ueda K, Okamoto K. Chem Mater 2002:14:4654:
  - Ray SS, Maiti P, Okamoto M, Yamada K, Ueda K. Macromolecules 2002;35:3104;
  - Ray SS, Yamada K, Okamoto M, Ueda K. Polymer 2003;44:857; Ray SS, Yamada K, Okamoto M, Fujimoto Y, Ogami A, Ueda K. Polymer 2003;44:6633.
- [9] Paul MA, Alexandre M, Degee P, Henrist C, Rulmont A, Dubois P. Polymer 2003;44:443.
- [10] White LA. J Appl Polym Sci 2004;92:2125.
- [11] Ray SS, Okamoto K, Okamoto M. Macromolecules 2003;36:2355.
- [12] Lu J, Hong CK, Wool RP. J Polym Sci B Polym Phys 2002;42:1441.
- [13] Asira F. Adv Chitin Sci 2000;46:1.
- [14] Darder M, Colilla M, Ruiz-Hitzky E. Chem Mater 2003;15:
- [15] Kumar MNVR. React Funct Polym 2000;46:1.
- [16] Lucas BN, Oliver WC, Swindeman JE. Mater Res Soc Symp Proc 1998;522:3.
- [17] Krumova M, Flores A, Balta Calleja FJ, Fakirov S. Colloid Polym Sci 2002;280:591.
- [18] Beake BD, Chen S, Hull JB, Gao F. J Nanosci Nanotech 2002;2:73.
- [19] Samuels RJ. J Polym Sci Polym Phys Ed 1981;19:1081.
- [20] Ogawa K, Yui T, Miya M. Biosci Biothechnol Biochem 1992;56:858.
- [21] Tirkistani FAA. Polym Degrad Stab 1998;60:67.
- [22] Qu X, Wirsen A, Albertsson AC. Polymer 2000;41:4841.
- [23] Toffey A, Samaranayake G, Frazier CE, Glasser WG. J Appl Polym Sci 1996;60:75.
- [24] Wang SF, Hu Y, Song L, Wang ZZ, Cheng ZY, Fan WC. Polym Degrad Stab 2002;77:423.
- [25] Gilman JW. Appl Clay Sci 1999;15:31.
- [26] Vaia RA, Price G, Ruth PN, Nguyen HT, Lichtenhan J. Appl Clay Sci 1999;15:67–92.
- [27] Liu TX, Tjiu WC, He CB, Na SS, Chung TS. Polym Int 2004;53:392.
- [28] Shen L, Phang IY, Chen L, Liu TX, Zeng KY. Polymer 2004;45:3341.
- [29] Korsunsky AM, McGurk MR, Bull SJ, Page TF. Surf Coat Tech 1998:99:171.
- [30] Swain MV, Mencik J. Thin Solid Films 1994;253:204.
- [31] Nix WD, Gao HJ. Mech Phys Solids 1998;46:411.